Available online at www.sciencedirect.com

SCIENCE DIRECT

Biochimica et Biophysica Acta 1708 (2005) 250–261

BIOCHIMICA ET BIOPHYSICA ACTA BBA

http://www.elsevier.com/locate/bba

A cell-based model for the photoacclimation and CO_2-acclimation of the photosynthetic apparatus

I.A. Papadakis*, K. Kotzabasis, K. Lika

Department of Biology, University of Crete, GR-71409, Heraklion, Crete, Greece

Received 19 January 2005; received in revised form 28 February 2005; accepted 3 March 2005
Available online 24 March 2005

Abstract

We have developed a mathematical model based on the underlying mechanisms concerning the responses of the photosynthetic apparatus of a microalga cell which grows under constant incident light intensity and ambient CO_2 concentration. Photosynthesis involves light and carbon-fixation reactions which are mutually dependent and affect each other, but existing models for photosynthesis don't account for both reactions at once. Our modeling approach allows us to derive distinct equations for the rates of oxygen production, NADPH production, carbon dioxide fixation, carbohydrate production, and rejected energy, which are generally different. The production rates of the photosynthesis products are hyperbolic functions of light and CO_2 concentration. The model predicts that in the absence of photoinhibition, CO_2-inhibition, photorespiration, and chlororespiration, a cell acclimated to high light and/or CO_2 concentration has higher photosynthetic capacity and lower photosynthetic efficiency than does a cell acclimated to low conditions. This results in crossing between the two curves which represent the oxygen production rates and carbon fixation rates in low and high conditions. Finally, in the absence of photoinhibition and CO_2-inhibition, the model predicts the carbohydrate production rate in terms of both light intensity and CO_2 concentration.

Keywords: Photosynthesis; Light reaction; Carbon-fixation reaction; Mathematical model; Synthesizing unit

1. Introduction

Photosynthesis is one of the few anti-entropic mechanisms on Earth. It is a complicated photochemical process occurring in photosynthetic organisms and leads to the transformation of the photon to chemical energy. Nowadays, phytoplankton photosynthesis occurring in photobioreactors could be used not only for the production of organic carbon, such as carbohydrates and/or proteins, but also for the production of hydrogen and electricity [1–3]. In addition, phytoplankton could be used for the absorption of polluting carbon dioxide with the aim of controlling the greenhouse phenomenon. For these implementations, we must have a better understanding of the underlying mechanisms concerning the function and regulation of photosynthesis, in order to evaluate and organize the experimental observations and, ultimately, to model these processes and responses with the aim to predict the optimum combination of the involved factors for the growth and the production performance of phytoplankton photosynthetic organisms.

The process of photosynthesis can be distinguished into light and carbon-fixation reactions because they are physically separated. The two reactions can been described most easily as a sequence of events, but it should be kept in mind that these are interdependent processes [4]. Photosynthesis is obviously linked to the availability of light as well as to the availability of carbon dioxide. Although several cell-based models of photosynthesis have been proposed [5–13], they consider only the light availability and do not quantify the Calvin–Benson cycle (carbon-fixation reactions) directly. These models either use classic enzyme kinetics and assume slow enzyme-controlled reactions dependent only on light to account for the carbon-fixation reactions [5,8,11,13], or assume that photosynthetic rates are mainly

* Corresponding author. Fax: +30 2810 394408.
E-mail address: giapis@biology.uoc.gr (I.A. Papadakis).

0005-2728/$ - see front matter © 2005 Elsevier B.V. All rights reserved.
doi:10.1016/j.bbabio.2005.03.001

related to light intensity [9,11,12]. Other models recognize the CO_2 dependence but ignore it in the model [10] or assume that carbon fixation is proportional to the light intensity and the available carbon [14]. As the main novelty, in the present contribution, we directly model both light and carbon-fixation reactions and consider both light intensity and carbon dioxide concentration for the following reasons. First, dissolved inorganic carbon is a required compound for the Calvin–Benson cycle so we can't neglect it. Second, CO_2 concentration dramatically affects the responses of photosynthetic apparatus [15–19]. Third, the model could be easily modified and used for mixotrophic and/or heterotrophic stages of the microalgae organisms [15] or in combination with autotrophic stages and growth under diurnal light. Fourth, it is easy to extend the model and combine it with another model concerning the synthesis and degradation of other compounds such as proteins. Fifth, we aim in deriving distinct equations for oxygen, NADPH, and carbohydrates (products of photosynthesis) because they play different roles in the process of photosynthesis.

An important concept in the study of photosynthesis is the photosynthetic unit (PSU). Previous models assume that the photosynthetic unit is the minimal and simplest composite structure of the photosynthetic apparatus [4,11], which consists of the light harvesting complex (LHC), the two photosystems (PS II and PS I), the *cytb*$_6$*f* complex, and the ATPase. We slightly modify this assumption, focusing on the size of the antenna of each functional PSU, which determines the light absorption, and the number of the electron transport chains of the cell, which reduce $NADP^+$ to NADPH in order to transfer NADPH to the Calvin–Benson cycle and determine the number of the functional PSUs of the cell. We assume that each functional PSU consists of the light harvesting complex, the photosystems (one or more PS II, one or more PS I), the *cytb*$_6$*f* complex, and the ATPase, and uses one electron transport chain [20]. We focus mainly on the number of functional electron transport chains and not on the absolute number of photosystems. The reason we had to modify slightly the definition of the PSU is because the PS II to PS I ratio does not always equal to one [4], but depends on endogenous factors as well as on the environmental conditions under which the cell grows [16,17,21–24]. Many studies have demonstrated that light quality and intensity, temperature, salt stress and their combinations affect photosynthetic characteristics such as the PS I/PS II reaction center ratio, electron transport capacities of two photosystems, cyclic electron transport activity and fluorescence in cyanobacteria and green microalgae [16]. Furthermore, according to [4] "there are possible exchanges of electromagnetic energy between antenna serving different PSUs, as well as electron flow between similar electron carriers of different electron transport chains linking PS II and PS I reaction centers. Moreover, it is the combined photochemical events of all functional reaction centers that establishes the electrochemical gradients within the thylakoid membrane and are crucial to the regulation of overall photosynthetic events". The LHC contains a few hundred photosynthetic pigment molecules, and the antenna size is determined by the quality, the quantity, and the spatial distribution of these pigments [25,26]. The whole photosynthetic process is energy supported by ATP. For model simplicity, we quantify indirectly the synthesis and the use of ATP. This consideration and the estimation of the required ATP quantity are based on experimental evidence which show that the required ATP quantity depends on endogenous factors as well as on environmental growth conditions [17].

In the present study, we focus on the responses of the photosynthetic apparatus to photo- and CO_2-acclimation. Photoacclimation is a long-term adaptation of the photosynthetic apparatus to the available irradiance when irradiance is constant for a prolonged time period [13]. Photoacclimation involves a change in the balance between the synthesis and degradation of proteins and pigments and takes more than 30 min, typically several hours or even several days [27,28]. Photoacclimation is usually controlled on the level of gene transcription or translation [27,28], so it is also a species-specific dependent process [29]. A cell which is acclimated to low light intensity has a large antenna and a low photosynthetic capacity [21,27,28,30,31], while a high light acclimated cell has a small antenna and a high photosynthetic capacity [21,28,30–34]. CO_2-acclimation is a long-term adaptation of the photosynthetic apparatus to the available carbon dioxide when its concentration is kept constant for about 1 day [35], and concerns the effect of CO_2 concentration on the activity of carbonic anhydrase, the ATP production, the active transport of CO_2, the manipulation of intracellular polyamines, and the total biomass production [17–19,35]. For cells acclimated to low-CO_2 concentration, the activity of carbonic anhydrase requires extra ATP and the function of the "CO_2-concentration mechanism" enables cells to acquire a high affinity for CO_2 [17].

Our modeling approach is based on the Synthesizing Unit (SU) and the Carrier Synthesizing Unit (CSU) concepts [36,37] and not on classic enzyme kinetics. In its simplest form, the SU is an enzyme or a complex of enzymes that binds a substrate molecule to deliver a product or a set of product molecules. A carrier is a synthesizing unit with a specialized function: it receives substrate molecules from outside the cell, and delivers them to a set of SUs inside the cell. The main assumption of the SU concept is that each SU can be either in the binding stage, for a time period t_b, binding arrival substrate molecules with a fixed probability, or in the production stage, for a time period t_p, where no substrate molecules are accepted by the SU. At the end of the cycle period, $t_c = t_b + t_p$, a product or a set of products molecules are produced. The mean production rate, $\dot{J}_P$, of the SU is the inverse of the expected value of t_c, $\dot{J}_P = 1/\mathcal{E}\, t_c$; it is defined as the ratio of the cumulative number of events occurring in a large period to the length of that period.

2. The mathematical model of photosynthesis

The general structure of the photosynthesis model is shown in Fig. 1. The model includes the main pathways of both the light and carbon-fixation reactions. For our photosynthesis model, we consider three types of synthesizing units: the PSU (functional photosynthetic unit), the CO_2-carrier, and the CB-SU (Calvin–Benson synthesizing unit). Later in this section, we present more explanations about these SUs and their role in photosynthesis, but very briefly: light uptake occurs via the PSUs which are the machines that bind photons and produce oxygen, NADPH, and ATP (products of the light reactions); the CO_2-carrier quantifies the transportation of the ambient CO_2 molecules from the environment through the membrane of the cell to the CB-SU; and the CB-SU is the machinery which is associated with the carbon-fixation reactions of the photosynthesis that takes two supplementary compounds, CO_2 and NADPH, to produce carbohydrates. In the rest of this section, we provide the basic model equations of photosynthesis while their derivation is shown in the Appendix A. Table 1 lists the model variables and parameters.

2.1. Light reactions

We assume that light absorption occurs only in the functional photosynthetic units (PSUs). We assume that a PSU is the minimal and simplest functional composite structure of the photosynthetic apparatus which consists of the light harvesting complex (LHC), the photosystems (one or more PS II, one or more PS I), the *cytb*$_6$*f* complex, and the ATPase, and uses one electron transport chain. A PSU can be either at the binding stage and bind arriving photons with a certain probability ρ_L or at the production stage and no photons are bind. The value of the photon's binding probability ρ_L indicates the functional size of the antenna because the rate of light utilization by a photosystem is directly proportional to the light-harvesting antenna size [25]. Photons fall on the cell at a rate $\dot{J}_\Phi = N_A\, A_c\, I$, where N_A is the Avogadro number, A_c the surface area of the cell, and I the incident light intensity. A portion, $1-\sigma$, of these photons is lost, while the remaining photons arrive at the PSUs at a rate $\dot{J}_L$, given by

$$\dot{J}_L = \sigma N_A A_c I, \tag{1}$$

where σ is a light quality- and species-dependent parameter. The incident photons excite the photosynthetic pigments of the LHC and arrive via them to the reaction centers were activate the electron transport chain [4]. During this photochemical reaction, each PSU produces NADPH, ATP and

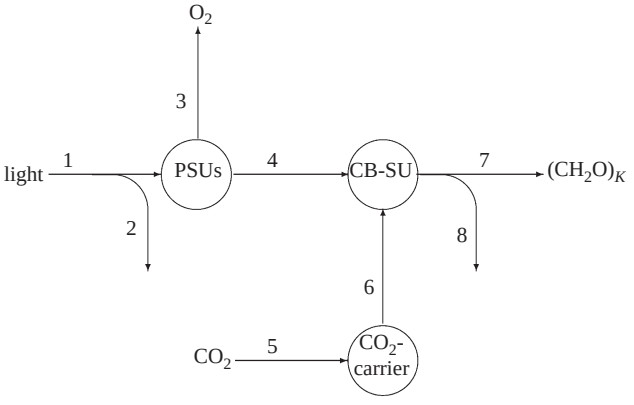

Fig. 1. Diagram of the photosynthesis model. Light and carbon dioxide are converted during light and carbon-fixation reactions by the synthesizing units (circles) into carbohydrates. Numbers indicate flux names: (1) rate of photon arrival to the PSUs ($\dot{J}_L$), (2) rate of rejected photons ($\dot{J}_{L,R}$), (3) rate of oxygen production ($\dot{J}_{O_2}$), (4) rate of NADPH production ($\dot{J}_N$), (5) rate of CO_2 absorption ($\dot{J}_{C,a}$), (6) rate of CO_2 arrival to the CB-SU ($\dot{J}_{C,p}$), (7) rate of carbohydrate net production ($\dot{J}_{CH}$), (8) rate of consumed carbohydrates ($(1-\epsilon)\,\dot{J}_{CH,t}$).

Table 1
Table of frequently used symbols

Symbol	Dim	Interpretation
I, I_K	mol hv l^{-2} t^{-1}	Incident light intensity, half saturation constant
X, X_K	mol CO_2 l^{-3}	CO_2 concentration, half saturation constant
$\dot{J}_\phi$, $\dot{J}_L$, $\dot{J}_{L,R}$	# hv t^{-1}	Incident, arrival, rejected rate of photons
$\dot{J}_{L,b}$, $\dot{J}_{L,m}$	mol t^{-1}	Binding, production rate by the PSU
$\dot{J}_{O_2}$, $\dot{J}_N$	mol t^{-1}	Production rate of oxygen, NADPH
$\{\dot{J}^m_{O_2}\}$, $\{\dot{J}^m_N\}$,	mol l^{-2} t^{-1}	Surface area-specific maximum production rate of oxygen, NADPH
$\dot{J}_{CH}$, $\dot{J}_{CH,t}$	mol t^{-1}	Net, total production rate of carbohydrates
$\{\dot{J}_{CH,m}\}$	mol l^{-2} t^{-1}	Surface area-specific carbohydrate monomer mean production rate
$\{\dot{J}_{C,m}\}$	mol l^{-2} t^{-1}	Surface area-specific CO_2 mean production rate by the CO_2-carrier
$\dot{J}_{C,a}$	mol t^{-1}	CO_2 arrival rate to the CO_2-carrier
$\dot{J}_{C,p}$	mol t^{-1}	CO_2 production rate by the CO_2-carrier
$\dot{J}_{C,b}$, $\dot{J}_{C,m}$	mol t^{-1}	Binding, production rate by the CO_2-carrier
A_c	l^2	Cell surface area
N_A	# mol^{-1}	Avogadro number
S	mol PSU	Functional PSUs per cell
$\{S\}$	mol PSU l^{-2}	Surface area-specific density of PSUs ($\{S\} \equiv S/A_C$)
σ	–	Photon's cellular cross section
n	–	Number of required photons to excite a PSU
$\dot{\zeta}$	l t^{-1}	CO_2's cellular cross section rate
K	–	Number of carbohydrate monomers
ρ_L	–	Photon's binding probability
ρ_C	–	CO_2 binding probability
λ_1	mol/mol	Cell's relative ability to CO_2 elaboration vs. photon's elaboration
λ_2	mol/mol	Cell's relative ability to carbon fixation vs. CO_2 molecules elaboration
ϵ	–	Efficiency of carbohydrate synthesis

Dots refer to rates (dimension: time^{-1}) and braces {} refer to quantities which are expressed per unit of surface area. In the dimension column, t means time, # number, and l means length.

oxygen. We assume that each PSU works as an one substrate-multi copy SU [36,37] which binds photons and produces NADPH and oxygen according to the chemical equation

$$4\ \mathrm{NADP} + 2\mathrm{H_2O} + n\mathrm{hv} \rightarrow 4\ \mathrm{NADPH} + \mathrm{O_2}.$$

We assume that photons arrive at a PSU according to a Poisson process and the PSU must bind n photons in order to enter the production stage. A microalga cell contains a large number, S, of PSUs, which work independently. From Eq. (14) follows that the mean photosynthetic oxygen production rate of a cell, $\dot{J}_{\mathrm{O_2}}$, in the absence of photorespiration and chlororespiration equals (see the Appendix A for details)

$$\dot{J}_{\mathrm{O_2}} = \left\{\dot{J}^{\mathrm{m}}_{\mathrm{O_2}}\right\} \frac{I}{I + I_{\mathrm{K}}} A_{\mathrm{c}}, \tag{2}$$

where $\{\dot{J}^{\mathrm{m}}_{\mathrm{O_2}}\} = \{S\}\dot{J}_{\mathrm{L,m}}$ is the maximum surface area-specific photosynthetic oxygen production rate, $I_{\mathrm{K}} = n\ \{S\}\ \dot{J}_{\mathrm{L,m}}\ \rho_{\mathrm{L}}^{-1}\ \sigma^{-1}$ the half saturation constant, $\{S\} = S/A_{\mathrm{c}}$ the surface area-specific density of PSUs, and $\dot{J}_{\mathrm{L,m}}$ the mean production rate of a PSU.

According to the above chemical equation and Eq. (2), the mean NADPH production rate of a cell, $\dot{J}_{\mathrm{N}}$, in the absence of photorespiration and chlororespiration equals

$$\dot{J}_{\mathrm{N}} = \left\{\dot{J}^{\mathrm{m}}_{\mathrm{N}}\right\} \frac{I}{I + I_{\mathrm{K}}} A_{\mathrm{c}}, \tag{3}$$

where $\{\dot{J}^{\mathrm{m}}_{\mathrm{N}}\} = 4\{S\}\dot{J}_{\mathrm{L,m}}$ is the maximum surface area specific NADPH production rate.

The photon's absorption occurs by the photosynthetic pigments during their excitation from the resting to the excited state. If all pigments are in the excited state, incident photons are rejected as fluorescence [4]. When photons arrive to a PSU, according to a Poisson process, the PSU returns a Poisson process of rejected photons. A large number of S PSUs will produce a Poisson stream of rejected photons at a rate which equals to the rate of incident photons onto the photosynthetic pigments of the cell, $\dot{J}_{\mathrm{L}}$, minus the rate of absorbed by the cell photons, $\dot{J}_{\mathrm{L,b}}$ [36,37]. Using Eqs. (1) and (13) from the Appendix A, we obtain that the rate of rejected by the cell photons, $\dot{J}_{\mathrm{L,R}}$, the so-called fluorescence, equals to

$$\dot{J}_{\mathrm{L,R}} = \sigma(1 - \rho_{\mathrm{L}}) N_{\mathrm{A}} A_{\mathrm{c}} I. \tag{4}$$

2.2. Carbon-fixation reactions

The photosynthetic carbohydrate production occurs during a sequence of complicated enzyme catalyzed reactions; that is, the Calvin–Benson cycle. These reactions are the well-known carbon-fixation reactions of the photosynthesis because they take place independently of the light presence using NADPH and ATP which are products of the light reactions. For modeling purposes, we assume that a microalga cell is one SU (we call it the Calvin–Benson Synthesizing Unit, CB-SU) which absorbs, in a parallel process, NADPH molecules from the S independent PSUs of the cell and CO_2 molecules from the one carbon dioxide carrier (CO_2-carrier) to produce carbohydrates. This process is energy supported with ATP molecules [4]. The CO_2-carrier quantifies the transportation of the ambient CO_2 molecules from the environment through the membrane of the cell to the CB-SU. The CO_2 transportation takes place either by diffusion, if the ambient CO_2 concentration is high, or with the aim of enzymes (energetic transportation), if the ambient CO_2 concentration is low. For a given ambient CO_2 concentration X, the CO_2 arrival rate to the CO_2-carrier, $\dot{J}_{\mathrm{C,a}}$, is taken to be proportional to the ambient CO_2 concentration [37], and the surface area of the cell

$$\dot{J}_{\mathrm{C,a}} = \dot{\zeta} A_{\mathrm{c}} X, \tag{5}$$

where $\dot{\zeta}$ is the cellular absorption cross section rate for carbon dioxide molecules and depends on environmental and endogenous factors. From Eq. (16) follows that the CO_2-carrier delivers CO_2 molecules to the CB-SU at a rate (see the Appendix A for details)

$$\dot{J}_{\mathrm{C,p}} = \left\{\dot{J}_{\mathrm{C,m}}\right\} \frac{X}{X + X_{\mathrm{K}}} A_{\mathrm{c}}, \tag{6}$$

where $\{\dot{J}_{\mathrm{C,m}}\}$, the surface area-specific CO_2 mean production rate by the CO_2-carrier, is species-specific and shows the cell's ability to CO_2 elaboration and $X_{\mathrm{K}} = \{\dot{J}_{\mathrm{C,m}}\}\ \rho_{\mathrm{C}}^{-1}\ \dot{\zeta}^{-1}$ is the half saturation constant.

The CB-SU absorbs one CO_2 molecule and four NADPH molecules and produces one carbohydrate monomer molecule, CH_2O. Every carbohydrate monomer molecule is fixated in the product of the previous CB-SU cycle according to the chemical equation

$$(\mathrm{CH_2O})_{(k-1)} + \mathrm{CO_2} + 4\ \mathrm{NADPH} \rightarrow (\mathrm{CH_2O})_k + \mathrm{H_2O} + 4\ \mathrm{NADP},$$

where $k = 1,2,\ldots,K$. The cycle is repeated K times sequentially for the production of one carbohydrate molecule. Substituting Eqs. (3) and (6) into (18) it follows that the total carbohydrate production rate of the cell is (see the Appendix A for details)

$$\dot{J}_{\mathrm{CH,t}} = \frac{\left\{\dot{J}_{\mathrm{CH,m}}\right\}}{K} A_{\mathrm{c}} \times \left[1 + \lambda_2 \left(4\lambda_1 \frac{I + I_{\mathrm{K}}}{I} + \frac{X + X_{\mathrm{K}}}{X} \times \left(1 + \lambda_1 \frac{\dfrac{X}{X + X_{\mathrm{K}}}}{\dfrac{I}{I + I_{\mathrm{K}}}}\right)^{-4}\right)\right]^{-1}, \tag{7}$$

where $\lambda_1 = \{\dot{J}_{\mathrm{C,m}}\} / \{\dot{J}^{\mathrm{m}}_{\mathrm{N}}\}$ is the cell's relative ability to CO_2 molecules elaboration versus photon's elaboration, $\lambda_2 = \{\dot{J}_{\mathrm{CH,m}}\} / \{\dot{J}_{\mathrm{C,m}}\}$ is the cell's relative ability to carbon molecules fixation versus CO_2 molecules elaboration, and $\{\dot{J}_{\mathrm{CH,m}}\}$ is the surface area-specific carbon fixation rate which is constant because it shows the cell ability to carbon fixation. We assume that the mean carbon-fixation time

interval, $\dot{J}_{\mathrm{CH,m}}^{-1}$, is the same for each cycle of the CB-SU because of the same biochemical process.

2.3. Cost for carbohydrate synthesis

The light and, mainly, the carbon-fixation reactions of photosynthesis are enzymatic and, by themselves, energy supported with ATP. The synthesis of the required enzymes, such as Rubisco, which are involved in these reactions is also energy supported with ATP. This energy demand is the cost for the carbohydrate synthesis and we model it indirectly assuming that it is proportional to the amount of the carbohydrates produced. So, a portion $(1-\epsilon)$ of the total amount of carbohydrate, $\dot{J}_{\mathrm{CH,t}}$, either has not been synthesized at all or it has been consumed in order to produce the equivalent amount of ATP necessary for the carbohydrate synthesis. For a cell growing under constant conditions, the energy cost for carbohydrate synthesis is constant and depends on the species. Therefore, the net carbohydrate production rate equals

$$\dot{J}_{\mathrm{CH}} = \epsilon \frac{\{\dot{J}_{\mathrm{CH,m}}\}}{K} A_{\mathrm{c}} \times \left[1 + \lambda_2 \left(4\lambda_1 \frac{I + I_{\mathrm{K}}}{I} + \frac{X + X_{\mathrm{K}}}{X} \times \left(1 + \lambda_1 \frac{\dfrac{X}{X + X_{\mathrm{K}}}}{\dfrac{I}{I + I_{\mathrm{K}}}}\right)^{-4}\right)\right]^{-1}. \quad (8)$$

3. Analysis and testing of the model

The oxygen production rate Eq. (2) and the NADPH production rate Eq. (3) have similar properties, thus, we will only discuss the first one. In the absence of photoinhibition, chlororespiration, and photorespiration, the mean oxygen production rate of the cell is a hyperbolic function of the light intensity, i.e., the curve is almost linear for low light intensities and leads to an asymptotic maximum for very high light intensities (the shape of the curve is as in Fig. 2), and it is also proportional to the surface area of the cell, A_{c}. The asymptotic maximum oxygen production rate of a cell with surface area A_{c} is

$$\lim_{I\to\infty} \dot{J}_{\mathrm{O_2}} = \left\{\dot{J}_{\mathrm{O_2}}^{\mathrm{m}}\right\} A_{\mathrm{c}} = \{S\}\dot{J}_{\mathrm{L,m}} A_{\mathrm{c}}. \quad (9)$$

For very low light intensities ($I \to 0$) the slope of Eq. (2) is

$$\lim_{I\to 0} \frac{\mathrm{d}\dot{J}_{\mathrm{O_2}}}{\mathrm{d}I} = \frac{\left\{\dot{J}_{\mathrm{O_2}}^{\mathrm{m}}\right\}}{I_{\mathrm{K}}} A_{\mathrm{c}} = \frac{\sigma}{n}\rho_{\mathrm{L}} A_{\mathrm{c}}. \quad (10)$$

3.1. Photoacclimation and CO_2-acclimation

A cell growing for a long time interval under a constant light intensity and a constant CO_2 concentration acclimates its photosynthetic mechanism to these conditions. These phenomena are known as photoacclimation and CO_2-acclimation, respectively. When the cell grows in a constant environment the photosynthetic surface area-specific maximum production rates, $\{\dot{J}_{\mathrm{O_2}}^{\mathrm{m}}\}$ and $\{\dot{J}_{\mathrm{N}}^{\mathrm{m}}\}$, are constant too. These quantities are independent of the cell size because they are expressed on a per surface area base and for constant growth conditions (e.g., constant light, temperature and salinity) they depend only on the species. We express these quantities on a per surface area base and not on a per volume base because the light absorption is associated with thylakoid-membrane surface. We assume that photoacclimation affects primarily the photon's binding probability ρ_{L} and the density $\{S\}$ of the PSUs, whereas CO_2-acclimation affects primarily the CO_2 binding probability ρ_{C} and the relative cost for carbohydrate synthesis $(1-\epsilon)$.

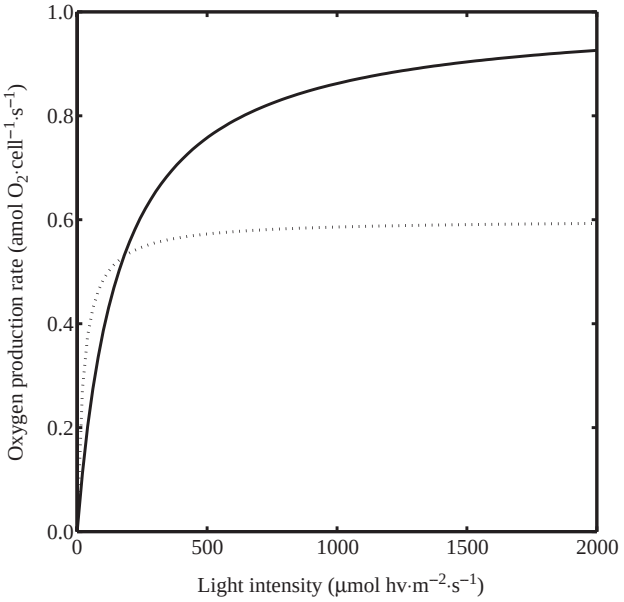

Fig. 2. PI curves according to Eq. (2). The solid curve represents high light (HL) photoacclimated cells and the dotted curve low light (LL) photoacclimated cells. Parameter values: $\{\dot{J}_{\mathrm{O_2}}^{\mathrm{m}}\}$=0.1 μmol O_2 m^{-2} s^{-1}, I_{K}=160 μmol hv m^{-2} s^{-1} for the HL-curve and $\{\dot{J}_{\mathrm{O_2}}^{\mathrm{m}}\}$=0.06 μmol O_2 m^{-2} s^{-1}, I_{K}=24 μmol hv m^{-2} s^{-1} for the LL-curve. For both HL and LL photoacclimated cells, we assume a mean surface area of the cell, A_{c}=10 μm^2.

A cell photoacclimated to low light has a large antenna, that is a large LHC-size, while a cell photoacclimated to high light has a small antenna, that is a small LHC-size [21,27,28,30,31]. We assume that the photon's binding probability ρ_{L} is proportional to the antenna's size; thus, the value of the parameter ρ_{L} will be high for LL and low for HL photoacclimated cells. Furthermore, there is evidence [38] that the number of the electron transport chains tends to be lower in LL photoacclimated plants than in HL photoacclimated plants; thus, we assume that the number of PSUs and, therefore, the density $\{S\}$ of the PSUs for LL photoacclimated cells is less than those acclimated to HL.

It follows from Eqs. (9) and (10) that the density of the PSUs, $\{S\}$, affects the asymptotic maximum of the photo-

synthetic oxygen production rate and the photon's binding probability, ρ_L, affects its slope at zero irradiance. Thus, the maximum production rate is low for LL and high for HL photoacclimated cells of the same size, while the slope at zero light intensity is steeper for LL than for HL photoacclimated cells with the same size. These properties of Eq. (2) lead to a crossing of the PI curves, and are shown in Fig. 2. Furthermore, the value of the half saturation irradiance constant, $I_K = n\ \{S\}\ \dot{J}_{L,m}\ \rho_L^{-1}\ \sigma^{-1}$, is low for LL and high for HL photoacclimated cells of the same size, since it is proportional to $\{S\}$ and inversely proportional to ρ_L.

Jin et al. [31], in an experiment, conducted to examine the involvement of zeaxanthin and Cbr protein in the repair of Photosystem II from photoinhibition in the green alga *Dunaliella salina*, measured the efficiency and productivity of photosynthesis in a wild-type *D. salina* as well as in a light-sensitive and chlorophyll-deficient mutant. They found that LL-grown wild-types and mutants had similar photosynthetic efficiencies, 0.40 and 0.42, respectively measured as the slope of the initial part of the photosynthesis–irradiance curve. However, when these types are grown under HL conditions, their photosynthetic efficiencies where reduced to 0.18 and 0.22, respectively. The photosynthetic capacity, i.e., the light-saturated rate of oxygen of the LL-grown mutant was 96.5 ± 1.2 mmol O_2 (mol Chl)$^{-1}$ s^{-1} and 70.0 ± 5.2 mmol O_2 (mol Chl)$^{-1}$ s^{-1} for the LL-grown wild-type. For the HL-grown cells, the photosynthetic capacities were more than 180 mmol O_2 (mol Chl)$^{-1}$ s^{-1} since photosynthesis did not yet saturate even at 3000 μmol photons m^{-2} s^{-1}. Note that the cells were acclimated at light intensities of 2000 μmol photons m^{-2} s^{-1} (HL) and 100 μmol photons m^{-2} s^{-1} (LL). In order to test the model against these observations, we have to transform Eq. (2) in terms of Chl. If λ is the number of mol Chl per cell, then $P \equiv \dot{J}^m_{O_2}/\lambda$ and $P_{max} \equiv \{\dot{J}^m_{O_2}\} A_C/\lambda$ are the oxygen production rate and the photosynthetic capacity, respectively, expressed in mmol O_2 (mol Chl)$^{-1}$ s^{-1} and $\phi \equiv P_{max}/I_K$ is the photon use efficiency. Therefore, Eq. (2) changes to $P = P_{max} I/(I + P_{max}/\phi)$. Fig. 3 shows the PI curves using the parameter values from [31].

If one is interested in the curvature of the PI curves for cells acclimated at different light conditions that appear to have similar maximum photosynthetic rates, one has to change the values of only two parameters, the photon's binding probability, ρ_L, and the density of PSUs, $\{S\}$, in order to fit the model (Eq. (2)) to these responses. Based on the model assumptions, these cells have similar densities of PSUs $\{S\}$, which increase as the growth irradiance increases and different photon's binding probabilities ρ_L, which decrease as the growth irradiance increases (Fig. 4A). These parameters depend on the photoacclimation state of the cell and are species specific. On the other hand, if one is interested in PI curves with significantly different maximum photosynthetic rates but similar slopes at zero irradiance, one can change the values of the same two parameters in the model. Cells that produce these type of PI curves have

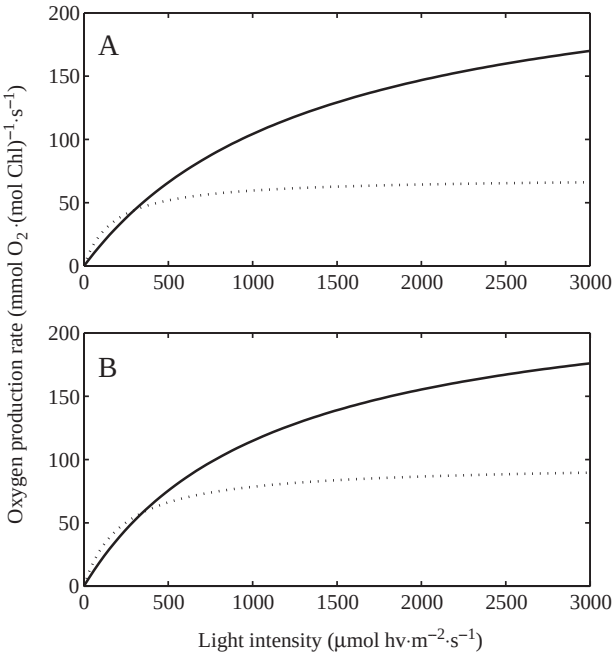

Fig. 3. PI curves according to Eq. (2) and parameter values from [31] (see text for details). The solid curves represent high light (HL) photoacclimated cells and the dotted curves low light (LL) photoacclimated cells. (A) Parameter values for wild-types: P_{max}=248 mmol O_2 m^{-2} (mol Chl)$^{-1}$ s^{-1}, ϕ=0.18 for the HL-curve and P_{max}=70 mmol O_2 m^{-2} (mol Chl)$^{-1}$ s^{-1}, ϕ=0.4 for the LL-curve. (B) Parameter values for mutants: P_{max}=240 mmol O_2 m^{-2} (mol Chl)$^{-1}$ s^{-1}, ϕ=0.22 for the HL-curve and P_{max}=96.5 mmol O_2 m^{-2} (mol Chl)$^{-1}$ s^{-1}, ϕ=0.42 for the LL-curve.

similar densities of PSUs $\{S\}$ and different photon's binding probabilities ρ_L (Fig. 4B). These types of responses have been experimentally observed [33,34] for cells of the chlorophyte *Dunaliella tertiolecta* and the diatom *Skeletonema costatum* (data are shown in Table 2).

The relationship between carbohydrate net production rate and availability of light and carbon dioxide is given by Eq. (8) and predicts the simultaneous dependence of carbohydrate production rate on light intensity and carbon dioxide concentration, in the absence of photoinhibition and CO_2-inhibition. To reduce the number of parameters, we nondimensionalize Eq. (8) by introducing the scaled variables $\dot{J}^*_{CH} = \dot{J}_{CH}/(\{\dot{J}_{CH,m}\} A_c/K)$, $I^* = I/I_K$, and $X^* = X/X_K$. Eq. (8) then becomes

$$\dot{J}^*_{CH} = \epsilon \left[1 + \lambda_2 \left(4\lambda_1 \frac{I^* + 1}{I^*} + \frac{X^* + 1}{X^*} \times \left(1 + \lambda_1 \frac{\dfrac{X^*}{X^* + 1}}{\dfrac{I^*}{I^* + 1}} \right)^{-4} \right) \right]^{-1}. \quad (11)$$

The scaled carbohydrate production rate, in the absence of photoinhibition and CO_2-inhibition, increases hyperboli-

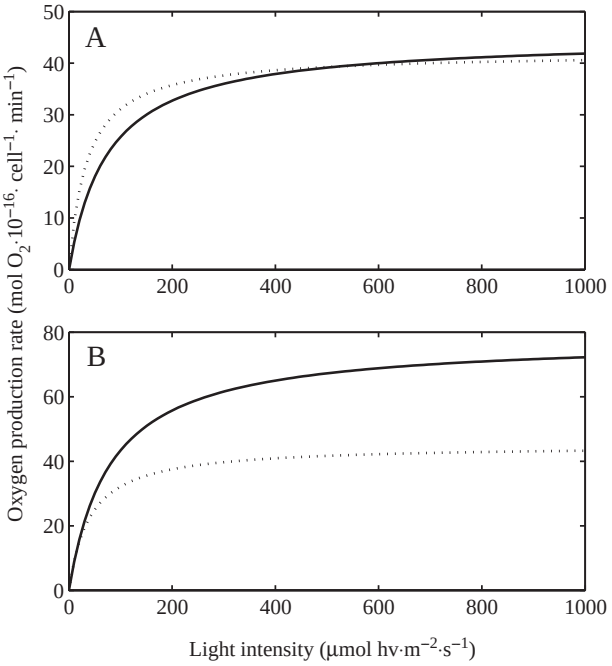

Fig. 4. PI curves for HL and LL photoacclimated cells with similar maximum photosynthetic rates (A) and similar initial slopes (B). The solid curves represent high light (HL) photoacclimated cells and the dotted curves low light (LL) photoacclimated cells. The parameter values were derived based on the data of [33] and [34] (see Table 2 and text for details). Parameter values: (A) $\{\dot{J}^{m}_{O_2}\}=45$ μmol O_2 m^{-2} min^{-1}, $I_K=75$ μmol hv m^{-2} s^{-1} for the HL-curve and $\{\dot{J}^{m}_{O_2}\}=42$ μmol O_2 m^{-2} min^{-1}, $I_K=35$ μmol hv m^{-2} s^{-1} for the LL-curve. (B) $\{\dot{J}^{m}_{O_2}\}=78$ μmol O_2 m^{-2} min^{-1}, $I_K=80$ μmol hv m^{-2} s^{-1} for the HL-curve and $\{\dot{J}^{m}_{O_2}\}=46$ μmol O_2 m^{-2} min^{-1}, $I_K=40$ μmol hv m^{-2} s^{-1} for the LL-curve. For all cells, we assume a mean surface area of the cell, $A_c=1.0\cdot10^{-10}$ m^2.

cally as both light intensity and carbon dioxide concentration increase (Fig. 5). It is almost linear for low light intensity and low carbon dioxide concentration, whereas saturates for high values of these variables.

For the production of carbohydrates, both NADPH and carbon dioxide are required. The mean binding period $\mathcal{E}_{t_b}$ of the two supplementary compounds, Eq. (17) in the Appendix A, shows how these compounds limit the synthesis of carbohydrates. For large values of the NADPH flux, $\dot{J}_N$, the mean binding period is $\mathcal{E}_{t_b}\approx\frac{1}{\dot{J}_{C,p}}$, i.e., the CO_2 acts as limiting factor for the carbohydrate synthesis. In this case, the carbohydrate net production rate quantifies as $\dot{J}_{CH}=(\epsilon/K)\ (\dot{J}^{-1}_{CH,m}+\dot{J}^{-1}_{C,p})^{-1}$, which after substituting Eq. (6), and in the absence of CO_2-inhibition, becomes $\dot{J}_{CH}=\frac{\epsilon\{\dot{J}_{CH,m}\}A_C}{K(1+\lambda_2)}\frac{X}{X+\frac{\lambda_2}{1+\lambda_2}X_K}$. The carbohydrate production rate is hyperbolic function of the CO_2 concentration, X, and proportional to the surface area of the cell, A_c. The properties of the equation for low CO_2-acclimated cells and high CO_2-acclimated cells are shown in Fig. 6A. The specific cost for carbohydrate synthesis, $(1-\epsilon)$, is high for low CO_2-acclimated cells because the active transport of carbon dioxide requires extra ATP due to the activity of carbonic anhydrase (CA) [17] and affects the asymptotic maximum

Table 2
Response of the photosynthetic capacity, P_{max}, to the growth irradiance, I_g, for *Dunaliella tertiolecta* and *Skeletonema costatum* cells

	I_g (μmol hv m^{-2} s^{-1})	P_{max} (mol O_2 10^{-16} $cell^{-1}$ min^{-1})
D. tertiolecta[1]	45	42
	600	45
S. costatum[1]	30	21
	200	21
	600	24
D. tertiolecta[2]	2	31
	8	38
	20	46
	60	65
	120	71
	200	74
	400	78
S. costatum[2]	0.7	3.1
	2.6	3.9
	9	7.4
	20	10.9
	39	15.1
	65	15.9
	130	15.8

Data from [34][1] and [33][2].

$\dot{J}^{m}_{C}=(\epsilon\dot{J}_{CH,m}A_c)/(1+\lambda_2)$ of the curve via the parameter ϵ. This maximum is lower for the low CO_2-acclimated cells than for high CO_2-acclimated cells. On the other hand, the active transport of CO_2 assures higher CO_2 binding probability ρ_C, and lower half saturation constant X_K for the low CO_2-acclimated cells which leads to a crossing of the curves [17]. For large values of the CO_2 flux, $\dot{J}_{C,p}$, the mean binding period is $\mathcal{E}_{t_b}\approx\frac{4}{\dot{J}_N}$, i.e., the NADPH acts as limiting factor for the carbohydrates synthesis. In this case, the carbohydrate net production rate quantifies as $\dot{J}_{CH}=(\epsilon/K)$ $(\dot{J}^{-1}_{CH,m}+4\ \dot{J}^{-1}_{N})^{-1}$. After substituting Eq. (6) follows that, in the absence of photoinhibition, the rate of carbohydrate net

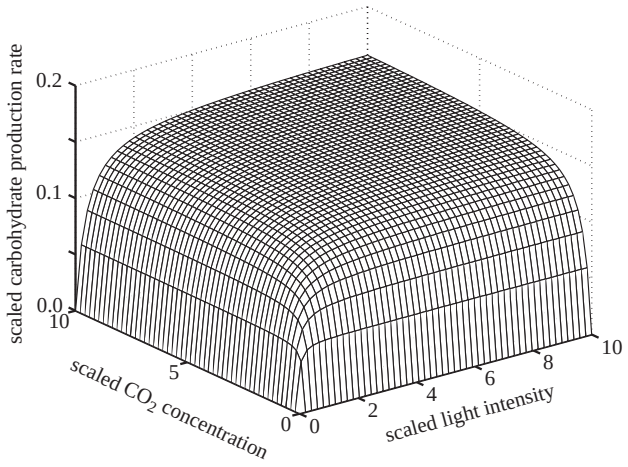

Fig. 5. Carbohydrate production rate as a function of light intensity and carbon dioxide in the absence of photoinhibition and CO_2-inhibition (scaled quantities). Parameter values: $\lambda_1=0.25$, $\lambda_2=1$, $\epsilon=0.4$.

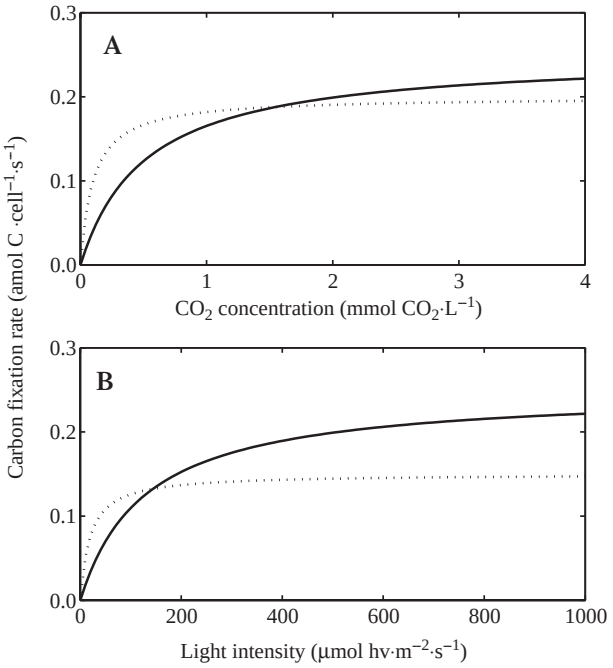

Fig. 6. The carbon fixation rate as (A) a function of carbon dioxide concentration, when NADPH is abundant, for cells acclimated to high-CO_2 (solid curve) and low-CO_2 (dotted curve) concentration and (B) as a function of light intensity, when CO_2 is abundant, for cells photoacclimated to high light (solid curve) and low light (dotted curve). Parameter values: (A) $\{\dot{J}_{CH,m}\}=0.1$ μmol C m^{-2} s^{-1}, $\lambda_2=1$, $X_K=1.0$ mM, $\epsilon=0.5$ for the high-CO_2 curve and $X_K=0.2$ mM, $\epsilon=0.4$ for the low-CO_2 curve. (B) $\epsilon=0.5$, $\lambda_1=0.25$, $\lambda_2=1$, $\{\dot{J}_{CH,m}\}=0.1$ μmol C m^{-2} s^{-1}, $I_K=160$ μmol hv m^{-2} s^{-1}, for the HL-curve and $\{\dot{J}_{CH,m}\}=0.06$ μmol C m^{-2} s^{-1}, $I_K=24$ μmol hv m^{-2} s^{-1}, for the LL-curve. For all cells we assume $A_c=1.0\cdot10^{-11}$ m^2.

production, in terms of light intensity is given by $\dot{J}_{CH}=\frac{\epsilon 4\lambda_1\lambda_2\{S\}\dot{J}_{L,m}A_C}{K(1+4\lambda_1\lambda_2)}\frac{I}{I+\frac{4\lambda_1\lambda_2}{1+4\lambda_1\lambda_2}I_K}=\frac{\epsilon\{\dot{J}_{CH,m}\}A_c}{K(1+4\lambda_1\lambda_2)}\frac{I}{I+\frac{4\lambda_1\lambda_2}{1+4\lambda_1\lambda_2}I_K}$.

A cell photoacclimated to LL has a higher value of the photon's binding probability ρ_L and a lower value of the density $\{S\}$ of the PSUs than a HL photoacclimated cell. The photon's binding probability, ρ_L, affects the initial slope of the carbon fixation rate curve $\alpha=\epsilon A_c\sigma\rho_L/n$, and the cell density of the PSUs, $\{S\}$, affects its asymptotic maximum $P_{max}=\epsilon 4\lambda_1\lambda_2\{S\}\dot{J}_{L,m}A_c)/(1+4\lambda_1\lambda_2)=(\epsilon\dot{J}_{CH,m}A_c)/(1+4\lambda_1\lambda_2)$. Thus, the maximum carbon fixation rate is low for LL and high for HL photoacclimated cells of the same size, while the slope at zero light intensity is steeper for LL than for HL photoacclimated cells with the same size. These properties leads to a crossing of the carbon fixation rate curves (Fig. 6B). Partensky et al. [29] in an experiment conducted to examine the photoacclimation of *Prochlorococcus* sp. (Prochlorophyta) strains isolated from the North Atlantic (SARG and NATL1) and the Mediterranean Sea (MED) measured the efficiency, α, and the capacity of photosynthesis, as maximum carbon fixation rate per cell, P_{max}, for the three strains growing under white light. They found that the maximum carbon fixation rate increases, and the initial slope of the curve decreases as the growth irradiance increases (data are shown on Table 3).

4. Discussion

We have developed a mechanistic mathematical model of photosynthesis that accounts directly for both the light and carbon-fixation reactions. In addition, both light intensity and carbon dioxide availability, two essential compounds for the process of photosynthesis, are input variables in our model. The model equations were derived from the synthesizing unit concept as proposed by [36,37]. This approach allows us to quantify the enzyme kinetics in terms of fluxes rather than concentrations as happens in classic enzyme kinetics study [5,39–49], which in turn, allows us to treat light as any chemical compound in the photochemical reactions [37]. Another advantage of this approach is that the coupling between the light and carbon-fixation reactions becomes easy. Furthermore, this model can be extended to include other compounds, such as N and Pi, and environmental parameters, such as salinity and temperature. This approach allowed us to develop a model that predicts separately the production rates of oxygen and NADPH, which are products of the light reactions, the rate of rejected light as fluorescence and the carbohydrate production rate, which is the product of the carbon-fixation reactions.

A simple model which incorporates both light and CO_2 in the dynamics of photosynthesis for higher plants [50], predicts only their short-term adaptation, is based on classic enzyme kinetics, and does not predict separately the photosynthetic products, but assumes that "the production ratio of CO_2 over O_2 can be taken to be 1". However, such an assumption contradicts the experimental evidence that the ratio of the mol C fixated per mol quanta of absorbed light varies depending on the species and the environmental growth conditions [29].

Other existing models, which also do not distinguish between the separate products of photosynthesis, assume that any photosynthesis-related productivity is similar and depends only on the incident light intensity [4–9,11,13,51,52]. These models neglect the direct impact of CO_2 in the photosynthetic process in order to avoid the

Table 3
Responses of the maximum carbon fixation rate, P_{max} (fg C cell^{-1} h^{-1}), and the photosynthetic efficiency, α (fg C cell^{-1} h^{-1} (μmol hv m^{-2} s^{-1})$^{-1}$), to the growth irradiance, I_g (μmol hv m^{-2} s^{-1}), in three *Prochlorococcus* sp. strains, MED, SARG, and NATL1, isolated from the North Atlantic and the Mediterranean Sea

Strain	I_g	α	P_{max}
MED	7.5	0.174	5.19
	16	0.062	4.91
	67	0.050	5.78
	133	0.073	5.85
SARG	7.5	0.234	2.76
	67	0.091	3.76
	133	0.073	6.23
NATL1	67	0.082	3.02
	133	0.059	4.17

Data from [29].

study of the Calvin–Benson cycle. Furthermore, the model developed by [13] is a complicated mechanistic model with some drawbacks, the worst of them being the violation of the energy conservation law; the model developed by [4] is a schematic empirical one, while other models are mainly stochastic, overcoming essential physiological and biochemical processes.

There are models which quantify the Calvin–Benson cycle [39,43,46,47,49] but, although they are considerably detailed in CO_2 fixation, neglect the impact of the light in photosynthetic reactions and its interaction and interdependence with the carbon-fixation reactions of photosynthesis. These models use classic enzyme kinetics, in terms of concentrations, neglected that the CO_2 transportation by diffusion and/or energetic transfer is a process which involves the membranes of the cell. In other words, the CO_2 transportation is a surface area- and not a volume-dependent process, so we must account not only for the concentrations inside and outside the cell but also the CO_2 transportation process through the membrane of the cell. Moreover, light reactions are surface area-dependent processes because they are localized within the thylakoid membranes, so a mechanistic model for the photosynthesis must consider the size of the cell. Only the present model, to the best of our knowledge, is in accordance with this consideration as each equation includes the surface area of the cell.

Fluorescence is a particular phenomenon with a great interest because it is coupled with the photosynthesis regulation mechanism [4] and it has never been mechanistically modeled. Observations show that fluorescence is proportional to the incident light intensity [4,21,27,28,32]. This model predicts that fluorescence increases with the light intensity (Eq. (4)) at which the microalga cell is exposed.

The present model accounts for the photoacclimation in the absence of photoinhibition, photorespiration, and chlororespiration. The major feature of our model, concerning photoacclimation, is the prediction that cells of the same size photoacclimated to low light have lower maximum production rate and half saturation irradiance constant than those photoacclimated to high light, while the slope of the PI curve and the carbon fixation rate curve at zero light intensity is steeper for low light photoacclimated than for high light photoacclimated cells. The crossing of the PI curves for cells acclimated to low and high light (Figs. 2–4, 6B) has been also experimentally observed [21,29,31–34,53,54]. It is a notable fact that [29] found, for two Atlantic unicellular algal strains grown under White Light (WL), that an increase in the photoacclimation irradiance was accompanied by a large increase in the maximum photosynthetic rate and a concomitant decrease in the initial slope of the PI curve when expressed either per cell or per Chl. This has also been observed in the prokaryote *Synechococcus* WH 7803 [53], in the unicellular green alga *D. salina* [31], and in the *Scenedesmus obliquus* [32]. Partensky et al. characterized this behavior quite atypical, because it does not fit any of the reported models for photosynthesis versus irradiance responses [29]. Unfortunately, not only models developed before 1993 [5,7,8,14] but more recently developed ones [9,11,13,52] do not fit to these observations also. The lack of fit of these models can be traced back to one assumption; they assume that the maximum photosynthetic rate decreases as the growth irradiance increases. Our model is the first, to the best of our knowledge, which supports this behavior. However, there are some experimentally determined curves expressed on a per cell basis which cannot be produced by the model in its present form, but note that the model does not yet include the impact of photorespiration, etc.

The present model also accounts for the CO_2-acclimation in the absence of CO_2-inhibition. Another feature of our model, concerning CO_2-acclimation, is the prediction that cells acclimated to low CO_2 concentration have lower maximum carbon fixation rate and half saturation constant than do those acclimated to high CO_2 concentration, while the slope of the carbon fixation rate versus CO_2 concentration curve is steeper for low CO_2-acclimated cells. The crossing of the carbon fixation rate versus CO_2 concentration curves for cells acclimated to low and high CO_2 concentration (Fig. 6A) has also been experimentally observed [17].

In the present study, we focus on the responses of the photosynthetic apparatus on photoacclimation and CO_2-acclimation under constant light intensity and CO_2 concentration. The model, in its present form, can be applied to variable conditions provided that such experimental data exist. Furthermore, the full potential of our modeling approach would be revealed when the model will be extended to include the effects of photo- and CO_2-adaptation, photo- and CO_2-inhibition, photorespiration, and chlororespiration. This work is currently under investigation.

Appendix A

In this appendix, we give the derivation of the model equations associated with the light and carbon-fixation reactions.

A.1. Light reactions

We assume that photons arrive at the functional PSUs according to a Poisson process at a rate $\dot{J}_L$. A PSU can be in a binding or in a production stage and it requires n photons to produce a product molecule. Let the binding period of one photon be exponentially distributed random variable with mean $\dot{J}_{L,b}^{-1}$. Then the binding period of the n photons, which is the sum of n independent exponential random variables with parameter $\dot{J}_{L,b}$, follows the Erlangian distribution [55] and has a mean value of $\mathcal{E}_{t_b} = n\dot{J}_{L,b}^{-1}$.

Let now the production period of one PSU be also an exponentially distributed random variable with mean $\dot{J}_{\mathrm{L,m}}^{-1}$. A single PSU produces the product Y (molecules of oxygen or NADPH for the light reactions) at a rate $\dot{J}_{\mathrm{Y}}=(\dot{J}_{\mathrm{L,m}}^{-1}+n\ \dot{J}_{\mathrm{L,b}}^{-1})^{-1}$, while a large set of S functional PSUs will produce a Poisson stream of product molecules at a rate (see pp. 44–45 in [37])

$$\dot{J}_{\mathrm{Y}}=\left(\left(s\dot{J}_{\mathrm{L,m}}\right)^{-1}+n\dot{J}_{\mathrm{L,b}}^{-1}\right)^{-1}. \tag{12}$$

When the photons arrive at a rate $\dot{J}_{\mathrm{L}}$, given by Eq. (1), and the photon binding probability is ρ_{L}, if the PSU is not in the production stage, then the mean binding photon rate is

$$\dot{J}_{\mathrm{L,b}}=\rho_{\mathrm{L}}\dot{J}_{\mathrm{L}}=\rho_{\mathrm{L}}\sigma N_{\mathrm{A}}A_{\mathrm{c}}I. \tag{13}$$

Substituting Eq. (13) (after converting it in mol hv per time) into Eq. (12), we find that the production rate of Y molecules is

$$\dot{J}_{\mathrm{Y}}=S\dot{J}_{\mathrm{L,m}}\frac{I}{I+nS\dot{J}_{\mathrm{L,m}}(\rho_{\mathrm{L}}\sigma A_{\mathrm{c}})^{-1}}. \tag{14}$$

A.2. Carbon-fixation reactions

During the carbon-fixation reactions two types of synthesizing units are involved: (1) the CB-SU, which uses two supplementary substrates, CO_2 and NADPH, to produce one product, carbohydrates, and (2) the CO_2-carrier, which transports the CO_2 from the environment to the CB-SU.

The CO_2-carrier can be either at the binding stage, and bind arrival CO_2 molecules with a certain probability ρ_{C} or at the production stage, and no CO_2 molecules are bind. We assume that CO_2 molecules arrive at the CO_2-carrier according to a Poisson process at a rate $\dot{J}_{\mathrm{C,a}}$, given (Eq. (5)). Then the CO_2 binding rate of the CO_2-carrier equals

$$\dot{J}_{\mathrm{C,b}}=\rho_{\mathrm{C}}\dot{J}_{\mathrm{C,a}}=\rho_{\mathrm{C}}\dot{\zeta}A_{\mathrm{c}}X. \tag{15}$$

Let the binding and the production periods, t_{b} and t_{p}, be exponentially distributed random variables, with means $\dot{J}_{\mathrm{C,b}}^{-1}$ and $\dot{J}_{\mathrm{C,m}}^{-1}$, respectively. The cycle period, t_{C}, of the CO_2-carrier concatenates one binding period and the subsequent production period, so the mean production rate of the CO_2-carrier, $\dot{J}_{\mathrm{C,p}}$, is the inverse of the expected value of t_{C}, i.e., $\dot{J}_{\mathrm{C,p}}=(\dot{J}_{\mathrm{C,b}}^{-1}+\dot{J}_{\mathrm{C,m}}^{-1})^{-1}$, which after substituting $\dot{J}_{\mathrm{C,b}}$ from Eq. (15) yields

$$\dot{J}_{\mathrm{C,p}}=\dot{J}_{\mathrm{C,m}}\frac{X}{\dot{J}_{\mathrm{C,m}}\left(\rho_{\mathrm{C}}\dot{\zeta}A_{\mathrm{c}}\right)^{-1}+X}. \tag{16}$$

The CO_2-carrier delivers CO_2 molecules and the PSUs deliver NADPH molecules, the supplementary substrate, to the CB-SU, in a parallel process. The CB-SU requires one CO_2 molecule and four NADPH molecules to produce one carbohydrate monomer molecule. The CB-SU will not bind molecules of a certain substrate, either because it already bound the required molecules of that substrate, but it still has to bind the other type of substrate, or because the CB-SU is in the production stage. Suppose that the binding of one substrate does not interfere with that of the other and let t_{b1} be the time of binding of the one CO_2 molecule and t_{b2} the time of binding of the fourth NADPH molecule. The random variables t_{b1} and t_{b2} follow the Erlangian distribution, $\phi(t;n,\lambda)=[\lambda(\lambda t)^{n-1}/(n-1)!]\exp\{-\lambda t\}$, with parameters $(1,\dot{J}_{\mathrm{C,p}})$ and $(4,\dot{J}_{\mathrm{N}})$, respectively.

The binding process is constraint by the minimum process rate, or else, by the maximum process time; that is, the time when all required substrate molecules are bound is $t_{\mathrm{b}}=\max\{t_{\mathrm{b1}},t_{\mathrm{b2}}\}$. The distribution function of t_{b} equals the product of the distribution functions of the independent random variables t_{b1} and t_{b2}. That is (see also pp. 45–48 in [37] for the general approach),

$$\Phi_{t_{\mathrm{b}}}(t)=\left(1-\exp\left\{-\dot{J}_{\mathrm{C,p}}t\right\}\right)\left(1-\sum_{i=0}^{3}\frac{\left(\dot{J}_{\mathrm{N}}t\right)^{i}}{i!}\exp\left\{-\dot{J}_{\mathrm{N}}t\right\}\right).$$

The expected value of the binding period is $\mathcal{E}_{t_{\mathrm{b}}}=\int_0^{\infty}(1-\Phi_{t_{\mathrm{b}}}(t))\mathrm{d}t$, which after some algebra yields

$$\mathcal{E}_{t_{\mathrm{b}}}=\frac{4}{\dot{J}_{\mathrm{N}}}+\frac{1}{\dot{J}_{\mathrm{C,p}}}-\sum_{i=0}^{3}\frac{\dot{J}_{\mathrm{N}}^{i}}{\left(\dot{J}_{\mathrm{N}}+\dot{J}_{\mathrm{C,p}}\right)^{i+1}}. \tag{17}$$

The expected value of one cycle period of the CB-SU is $\mathcal{E}_{t_{\mathrm{c}}}=\dot{J}_{CH,\mathrm{m}}^{-1}+\mathcal{E}_{t_{\mathrm{b}}}$, where $\dot{J}_{\mathrm{CH,m}}^{-1}$ is the mean carbon-fixation interval for one cycle of the CB-SU. After K sequential cycles, the mean carbohydrate production rate of the CB-SU, equals

$$\dot{J}_{\mathrm{CH,t}}=\frac{1}{K}\left(\dot{J}_{\mathrm{CH,m}}^{-1}+\frac{4}{\dot{J}_{\mathrm{N}}}+\frac{1}{\dot{J}_{\mathrm{C,p}}}-\sum_{i=0}^{3}\frac{\dot{J}_{\mathrm{N}}^{i}}{\left(\dot{J}_{\mathrm{N}}+\dot{J}_{\mathrm{C,p}}\right)^{i+1}}\right)^{-1}. \tag{18}$$

Acknowledgments

We are grateful to Prof. S.A.L.M. Kooijman for his valuable comments on an earlier version of the manuscript. We wish to thank the two anonymous referees for their substantial comments, and Dr. C. Zonneveld, Dr. E. Navakoudis, and N. Ioannidis for stimulating discussions at the start of this research. This research is part of the Ph. D. thesis of I.A. Papadakis.

References

[1] A. Melis, L. Zhang, M. Forestier, M. Chirardi, M. Seibert, Sustained photobiological hydrogen gas production upon reversible inactivation of oxygen evolution in the green alga *Chlamydomonas reinhardtii*, Plant Physiol. 122 (2000) 127–135.

[2] T. Kondo, M. Arakawa, T. Wakayama, J. Miyake, Hydrogen production by combining two types of photosynthetic bacteria

with different characteristics, Int. J. Hydrogen Energy 27 (2002) 1303–1308.
[3] T. Laurinavichene, I.V. Tolstygina, R.R. Galiulina, M.L. Ghirardi, M. Seibert, A.A. Tsyganov, Dilution methods to deprive *Chlamydomonas reinhardtii* cultures of sulfur for subsequent hydrogen photoproduction, Int. J. Hydrogen Energy 27 (2002) 1245–1249.
[4] B.B. Prézelin, Light reactions in photosynthesis, Can. J. Fish. Aquat. Sci. 210 (1981) 1–43.
[5] M.J.R. Fasham, T. Platt, Photosynthetic response of phytoplankton to light: a physiological model, Proc. R. Soc. Lond., B Biol. Sci. B 219 (1983) 355–370.
[6] R.O. Megard, D.W. Tonkyn, W.H. Senft, Kinetics of oxygenic photosynthesis in planktonic algae, J. Plankton Res. 6 (1984) 325–337.
[7] P.H.C. Eilers, J.C.H. Peeters, A model for the relationship between light intensity and the rate of photosynthesis in phytoplankton, Ecol. Model. 42 (1988) 199–215.
[8] P.H.C. Eilers, J.C.H. Peeters, Dynamic behaviour of a model for photosynthesis and photoinhibition, Ecol. Model. 69 (1993) 113–133.
[9] C. Zonneveld, Modeling effects of photoadaptation on the photosynthesis–irradiance curve, J. Theor. Biol. 186 (1997) 381–388.
[10] C. Zonneveld, H.A. van Den Berg, S.A.L.M. Kooijman, Modeling carbon cell quota in light-limited phytoplankton, J. Theor. Biol. 188 (1997) 215–226.
[11] C. Zonneveld, Photoinhibition as affected by photoacclimation in phytoplankton: a model approach, J. Theor. Biol. 193 (1998) 115–123.
[12] C. Zonneveld, A cell-based model for the chlorophyll α to carbon ratio in phytoplankton, Ecol. Model. 113 (1998) 55–70.
[13] C.F. Rubio, F.G. Camacho, J.M.F. Sevilla, Y. Chisti, E.M. Grima, A mechanistic model of photosynthesis in microalgae, Biotechnol. Bioeng. 81 (2003) 459–473.
[14] B. Shuter, A model of physiological adaptation in unicellular algae, J. Theor. Biol. 78 (1979) 519–552.
[15] A. Theodoridou, D. Dörnemann, K. Kotzabasis, Light-dependent induction of strongly increased microalgal growth by methanol, Biochim. Biophys. Acta 1573 (2002) 189–198.
[16] A. Satoh, N. Kurano, H. Senger, S. Miyachi, Regulation of energy balance in photosystems in response to changes in CO_2 concentrations and light intensities during growth in extremely-high-CO_2-tolerant green microalgae, Plant Cell Physiol. 43 (4) (2002) 440–451.
[17] S. Miyachi, I. Iwasaki, Y. Shiraiwa, Historical perspective on microalgal and cyanobacterial acclimation to low- and extremely high-CO_2 conditions, Photosynth. Res. 77 (2003) 139–153.
[18] J.L.F. Gordillo, C. Jiménez, F.L. Figueroa, X. Niell, Influence of elevated CO_2 and nitrogen supply on the carbon assimilation performance and cell composition of the unicellular alga *Dunaliella viridis*, Physiol. Plant. 119 (2003) 513–518.
[19] K. Logothetis, S. Dakanali, N. Ioannidis, K. Kotzabasis, The impact of high CO_2 concentrations on the structure and function of the photosynthetic apparatus and the role of polyamines, J. Plant Physiol. 161 (2004) 715–724.
[20] D.R. Ort, C.F. Yocum, Electron transfer and energy transduction in photosynthesis: an overview, in: D.R. Ort, C.F. Yocum (Eds.), Oxygenic Photosynthesis: The Light Reactions, Kluwer Academic Publishers, Dordrcht, 1996, pp. 1–9.
[21] M. Havaux, G. Guedeney, Q. He, A.R. Grossman, Elimination of high-light-inducible polypeptides related to eukaryotic chlorophyll *a*/*b*-binding proteins results in aberrant photoacclimation in *Synechocystis* pcc6803, Biochim. Biophys. Acta 1557 (2003) 21–33.
[22] A.N. Glazer, A. Melis, Photochemical reaction centers: structure, organization, and function, Annu. Rev. Plant Physiol. 38 (1987) 11–45.
[23] A. Melis, Dynamics of photosynthetic membrane composition and function, Biochim. Biophys. Acta 1058 (1991) 87–106.
[24] A. Melis, A. Murakami, J.A. Nemson, K. Aizawa, K. Ohki, Y. Fujita, Chromatic regulation in *Chlamydomonas reinhardtii* alters photosystem stoichiometry and improves the quantum efficiency of photosynthesis, Photosynth. Res. 47 (1996) 253–265.
[25] A. Melis, Excitation energy transfer: functional and dynamic aspects of lhc (cab) proteins, in: D.R. Ort, C.F. Yocum (Eds.), Oxygenic Photosynthesis: The Light Reactions, Kluwer Academic Publishers, Dordrcht, 1996, pp. 523–538.
[26] J.E.W. Polle, S. Kanakagiri, A. Melis, *tla1*, a DNA insertional transformant of the green alga *Chlamydomonas reinhardtii* with a truncated light-harvesting chlorophyll antenna size, Planta 217 (2003) 49–59.
[27] H. Dau, Short-term adaptation of plants to changing light intensities and its relation to Photosystem II photochemistry and fluorescence emission, J. Photochem. Photobiol. 26 (1994) 3–27.
[28] T. Masuda, J.E.W. Polle, A. Melis, Biosynthesis and distribution of chlorophyll among the photosystems during recovery of the green alga *Dunaliella salina* from irradiance stress, Plant Physiol. 128 (2002) 603–614.
[29] F. Partensky, N. Hoepffner, W.K.W. Li, O. Ulloa, D. Vaulot, Photoacclimation *Prochlorococcus* sp. (prochlorophyta) strains isolated from the North Atlantic and the Mediterranean Sea, Plant Physiol. 101 (1993) 285–296.
[30] K. Kotzabasis, B. Strasser, E. Navakoudis, D. Döernemann, The regulatory role of polyamines in structure and functioning of the photosynthetic apparatus during photoadaptation, J. Photochem. Photobiol., B Biol. 50 (1999) 45–52.
[31] E. Jin, J. Polle, A. Melis, Involvement of zeaxanthin and of the cbr protein in the repair of Photosystem II from photoinhibition in the green alga *Dunaliella salina*, Biochim. Biophys. Acta 1506 (2001) 244–259.
[32] K. Kotzabasis, D. Döernemann, Differential changes in the photosynthetic pigments and polyamine content during photoadaptation and photoinhibition in the unicellular green alga *Scenedesmus oblicuus*, Z. Naturforsch. 53c (1998) 833–840.
[33] G.P. Falkowski, T.G. Owens, A.C. Ley, D.C. Mauzerall, Effects of growth irradiance levels on the ratio of reaction centers in two species of marine phytoplankton, Plant Physiol. 68 (1981) 969–973.
[34] G.P. Falkowski, T.G. Owens, Light-shade adaptation. Two strategies in marine phytoplankton, Plant Physiol. 66 (1980) 592–595.
[35] S. Miyachi, J. Bürger, K. Kotzabasis, J. Thielmann, H. Senger, Photosynthetic characteristics of three strains of cyanobacteria grown-under low- or high-CO_2 conditions, Z. Naturforsch. 51c (1996) 40–46.
[36] S.A.L.M. Kooijman, The synthesizing unit as a model for the stoichiometric fusion and branching of metabolic fluxes, Biol. Chem. 73 (1998) 179–188.
[37] S.A.L.M. Kooijman, Dynamic Energy and Mass Budgets in Biological Systems, Cambridge University Press, Cambridge, 2000.
[38] J.M. Anderson, W.S. Chow, D.J. Goodchild, Thylakoid membrane organization in sun/shade acclimation, Aust. J. Plant Physiol. 15 (1988) 11–26.
[39] G. Pettersson, Error associated with experimental flux control coefficient determinations in the Calvin cycle, Biochim. Biophys. Acta 1289 (1996) 169–174.
[40] G. Pettersson, A new approach for determination of the selectivity favoured kinetic design of enzyme reactions, J. Theor. Biol. 183 (1996) 179–183.
[41] G. Pettersson, Errors associated with experimental determinations of enzyme flux control coefficients, J. Theor. Biol. 179 (1996) 191–197.
[42] G.L. Ngo, M.R. Roussel, A new class of biochemical oscillator models based on competitive binding, Eur. J. Biochem. 245 (1997) 182–190.
[43] G. Pettersson, Control properties of Calvin photosynthesis cycle at physiological carbon dioxide concentrations, Biochim. Biophys. Acta 1322 (1997) 173–182.
[44] E.L. Fridlyand, R. Scheibe, Controlled distribution of electrons between acceptors in chloroplasts: a theoretical consideration, Biochim. Biophys. Acta 1413 (1999) 31–42.
[45] G. Pettersson, Effect of dynamic channelling on the transient-state kinetics of coupled enzyme reactions, J. Theor. Biol. 198 (1999) 135–141.

[46] G.M. Poolman, D.A. Fell, S. Thomas, Modelling photosynthesis and its control, J. Exp. Bot. 51 (2000) 319–328.
[47] G.M. Poolman, H. Ölcer, J.C. Lioyd, C.A. Raines, D.A. Fell, Computer modelling and experimental evidence for two steady states in the photosynthetic Calvin cycle, Eur. J. Biochem. 268 (2001) 2810–2816.
[48] A. Cornish-Bowden, M.L. Cárdenas, Information transfer in metabolic pathways. Effects of irreversible steps in computer models, Eur. J. Biochem. 268 (2001) 6616–6624.
[49] G.M. Poolman, D.A. Fell, C.A. Raines, Elementary modes analysis of photosynthate metabolism in the chloroplast stroma, Eur. J. Biochem. 270 (2003) 430–439.
[50] S.O.M. Massunaga, C.N. Gatts, A.G. Gomes, H. Vargas, A simple model for the dynamics of photosynthesis, Anal. Sci. 17 Special Issue (2001) s29–s30.
[51] W.K. Dodds, B.J.F. Biggs, R.L. Lowe, Photosynthesis-irradiance patterns in benthic microalgae: variations as a function of assemblage thickness and community structure, J. Phycol. 35 (1999) 42–53.
[52] B.-P. Han, Photosynthesis-irradiance response at physiological level: a mechanistic model, J. Theor. Biol. 213 (2001) 121–127.
[53] T.M. Kana, P.M. Glibert, Effect of irradiances up to 2000 $\mu Em^{-2}s^{-1}$ on marine *Synechococcus* wh7803-ii. Photosynthetic responses and mechanisms, Deep-Sea Res. 10 (1987) 497–516.
[54] C.E. Payri, S. Maritorena, C. Bizeau, M. Rodiére, Photoacclimation in the tropical alga *Hydrolithon onkodes* (Rhodophyta, corallinaceae) from French Polynesian reef, J. Phycol. 37 (2001) 223–234.
[55] R. Nelson, Probability, Stochastic Processes, and Queueing Theory, Springer-Verlag, New York, 1995.